

Using Smart Climate-Based Technology to Predict Water Availability in a Volcanic Landscape of Central Java, Indonesia – A Pathway to Conservation Strategy

Nur Ainun Harlin Jennie Pulungan^{1*}, Jihan Dwi Islami¹,
Andi Syahid Muttaqin¹, Junun Sartohadi¹

¹ Department of Soil, Faculty of Agriculture, Universitas Gadjah Mada, Yogyakarta, Indonesia

* Corresponding author's e-mail: nurainun.pulungan@ugm.ac.id

ABSTRACT

High need for precision agriculture today has been associated with the completeness of the data available. The application of smart technology becomes the main alternative for fulfilling incomplete data and predicting future data. This paper presents the results of a research that aims to monitor and to predict water availability for determining conservation strategy on water availability using time series data from satellite rainfall, spanning from 2007 to 2022. We employed the innovative use of remote sensing technology, global rainfall measurement (GPM) and Climate Hazards Group InfraRed Rainfall with Station data (CHIRPS), to assess and correct satellite-derived rainfall estimates against ground-based observations. Conducted in the Serang watershed of Mount Merbabu's volcanic landscape, the research employs a quantitative descriptive approach. We used coupled climate models MIROC6 and MRI-ESM2-0 in the CMIP-6 Framework for rainfall projections 2023–2030, then continued with the F.J. Mock model simulations for water availability projection. Our findings reveal a significant impact of climate change on water availability over the decade, with the most extreme conditions observed in 2029 and 2030, where the increasing of water availability reaching 10 m³/s. The results showed that CHIRPS performed well in describing rainfall data. The novelty of this research highlighting the potential of: firstly, the use of satellite rainfall data for this specific region has not been extensively studied before; secondly, the discovered impacts of climate change to the water availability are particularly noteworthy, and thus contributing to the sustainability of agricultural practices in response to climate change. A limitation of this study is the short investigation period of just one decade, which does not fully capture the long-term impacts of climate change. Future research is recommended to utilize satellite data over extended periods to better represent extreme climate events and derive drought and wetness patterns over durations exceeding one decade.

Keywords: climate-smart agriculture, rainfall projections, remote sensing technology, satellite rainfall data, Serang watershed, water availability.

INTRODUCTION

Rainfall data is the primary input required to predict weather conditions and hazard assessment such as flood, drought, and landslides. Many researches have studied related to these topics, e.g. [Ramzi et al., 2024; Ouharba et al., 2024; Tavosi, et al., 2024; Chellamuthu et al., 2024; Damayanti et al., 2022, Triyanto et al., 2021, Tabari, 2020; Stodolak et al., 2018]. Despite the high demand, the rainfall data lacks of its availability. It is difficult

to gain adequate ground-based observation rainfall data for further analysis. Mostly, for hydrological analysis, rainfall data is often obtained from direct observations in the field through rain gauges managed by certain agencies. However, in some areas, the measuring tools are not available. In other areas, the problem are the incomplete or empty rainfall data [Fauzi et al., 2013; Hasyimzoem et al., 2021]. And thus, it becomes a challenge. On the other side, rainfall data is also considered to be one of the most significant data

for agricultural needs. Rainfall is a source of water input for analysing regional water availability [Putri and Perdinan, 2018]. Dwiratna et al. [2014] used rainfall data to determine schedules and planting patterns for dryland agriculture, which are largely determined by the monthly rainfall conditions in the region due to their relation to meeting the water needs of plants. Rainfall data can also be used for agricultural planning, especially regarding the selection of appropriate commodities and potential cropping indices, which are highly dependent on the potential availability of existing water [Susanti et al., 2021]. Moreover, rainfall has a very close relationship with agricultural yields or production, as each plant has different climatological growth requirements. The relationship between rainfall and plant water balance is significantly influenced by climate anomaly events [Laimeheriwa et al., 2019; Simanjuntak et al., 2018].

Utilization of satellite rainfall data through remote sensing can overcome the challenges of rainfall data availability. Many studies explored the utilize of satellite rainfall data [Wu et al., 2024; Fadli, 2022; Partarini et al., 2021; Radhika et al., 2017; Fadholi et al., 2014]. Most of the existing rainfall studies explained the utilize of satellite rainfall data in a regional or global scale.

In this work, a research approach based on remote sensing for rainfall data requirements was presented and aimed to monitor and to predict the effect of climate change on water availability. The knowledge gap revealed in this research is that the use of satellite rainfall data for the specific region that has not been extensively studied before. In fact, for agricultural needs, the data in a specific region is mostly important regarding with the assessment of productivity per plot of land. This research introduces the alternative approach to gain rainfall data completely and detail. The methodological approach was complemented by field surveys and quantitative descriptive visual interpretation of satellite rainfall data. The implication of this study may contribute on reaching the sustainability of agricultural practices that can help to mitigate climate change impact.

METHODS

Study area

This research was conducted in the upper part of the Serang watershed, Central Java,

covering a study area of 282.81 km². This area serves as the recharge zone for the Serang watershed within the volcanic landscape of Mount Merbabu. Administratively, the majority of the study area is located in Boyolali Regency, with a small portion extending into Semarang Regency. The Serang watershed has an average slope of 11%, with the Serang River serving as the primary river, stretching over a main river length of 13.046 km [Romadhoniastri et al., 2022]. River discharge data were collected at the Guwo Water Post with an average river discharge of 10.33 m³/s. Figure 1 depicts the upper of the Serang watershed, highlighting the study area.

Data

This study utilizes rainfall data obtained from observation stations and satellites, supplemented by other datasets such as measured discharge data and CMIP-6 modeling data.

Station rain data (observation data)

Eight rain stations were used in this research: Juwangi, Karanggede, Simo, Sambu, Teras, Mojosoongo, Boyolali, and Ampel stations, providing a dataset spanning 16 years (2007–2022). Monthly rainfall data were acquired from the Boyolali District Office.

Satellite rain data

Global rainfall measurement (GPM) and Climate Hazards Group InfraRed Rainfall with Station (CHIRPS) satellite rainfall data were employed in this study. The selection of these datasets was based on previous research highlighting their accuracy [Yang et al., 2017; Liu et al., 2020]. The downloaded data length was adjusted to match the observed rainfall data, spanning 16 years. GPM data offer spatial resolution in a grid format of $0.10^\circ \times 0.10^\circ$ and are available in 3-hourly, daily, 5-day, and monthly periods. These data can be accessed via the website <https://gpm.nasa.gov/data/imerg>; alternatively, they can be downloaded from <https://giovanni.gsfc.nasa.gov/giovanni/> to obtain area-specific data. CHIRPS data provide a finer spatial resolution with a grid size of $0.05^\circ \times 0.05^\circ$ and offer data in daily, semi-monthly, and monthly periods. Global CHIRPS data can be accessed at <https://data.chc.ucsb.edu/products/CHIRPS-2.0/>. Area-specific data can be downloaded from Google Earth Engine. The downloaded grids for each satellite data are illustrated in Figure 2.

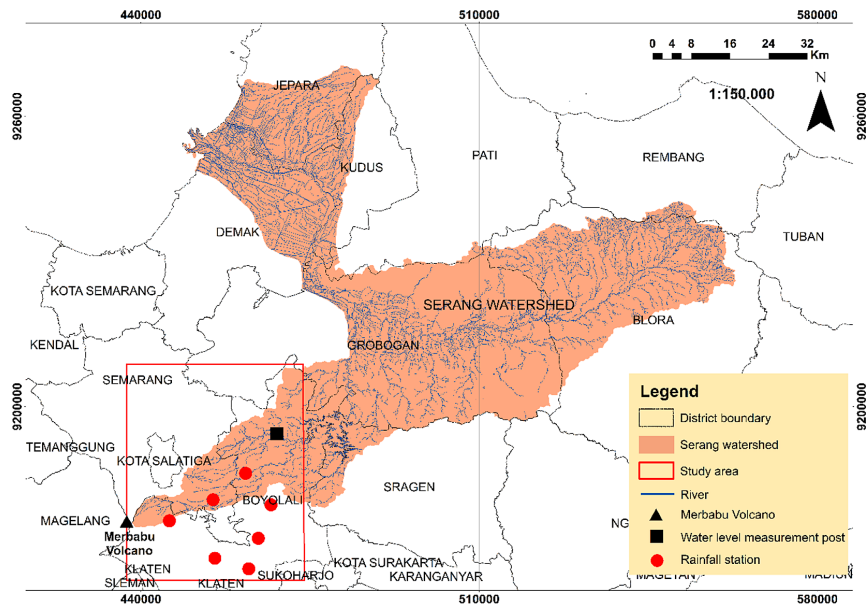


Figure 1. Study area: recharge area of Serang Watershed

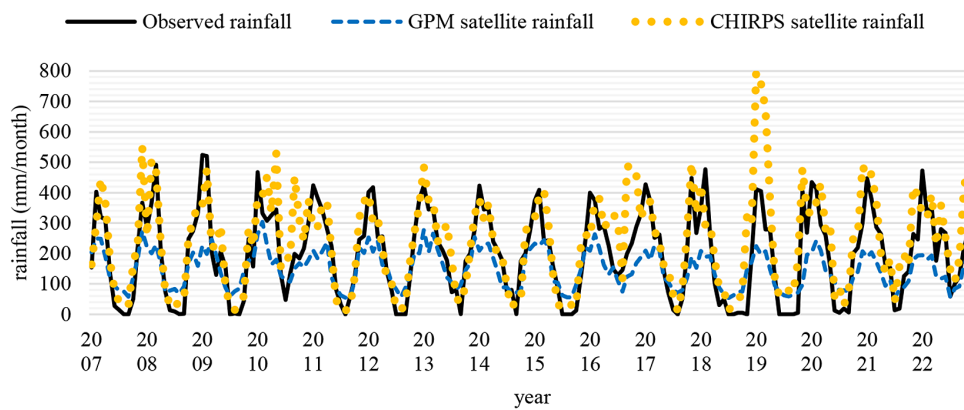


Figure 2. Comparative analysis of rainfall measurements: A comparison between observational data and satellite estimates (GPM and CHIRPS)

Projected rain data

CMIP-6 modeling was employed to obtain projected rainfall data from 2023 to 2030.

Measured discharge data

Discharge data were collected from Gowa Water Prediction Post, covering the period 2010–2020. These data utilized to calculate water availability predictions.

Analysis method

Satellite rain data processing typically involves of two primary stages: data calibration, which includes correcting the satellite rain data, and validation of the correction results. In this research, the data

processing is divided into two distinct phases based on the data timeframe. The calibration phase spans from 2007 to 2017, while validation is conducted using data from 2018 to 2022. It is a common practice in data correction to perform validation using data outside the calibration period [Indarto, 2012]. Monthly data intervals are utilized in this study for validation analysis, as this period is considered optimal for such analyses [Yang et al., 2017].

Correction of satellite rainfall data

Bias correction is intended to correct satellite rainfall values to match observed rainfall values. Bias correction in this study was carried out in two ways, i.e., regression method and distribution mapping method.

Regression method

In this study, the regression equations used are linear regression, exponential regression, and polynomial regression. These three equations will be used as corrections for satellite rainfall data. The equations used are Equations 1 to 3.

Linear regression: $\hat{Y} = aX + b$ (1)

Exponential regression: $\hat{Y} = b e^{ax}$ (2)

Polynomial regression:

$\hat{Y} = b_0 + b_1X + b_2X^2 + \dots + b_mX^m$ (3)

where: \hat{Y} – equation of the straight line Y (observed rainfall) to X (satellite rainfall), X – the independent variable in this case is satellite rainfall, a, b – regression coefficients, e – the base number of the original logarithm (Napir logarithm = 2.7183)

Distribution mapping method

The use of this method is carried out in several stages, namely identifying the type of probability distribution and rainfall probability. In this study, the normal distribution is the probability distribution method. The stage of determining the probability of rainfall is performed using the probability density function (PDF) and cumulative distribution function (CDF) with Equations 4 and 5 [Misnawati et al., 2018]. The probability density function (PDF) states the probability value of each event X and is written as $p(X)$. Because $p(X)$ expresses the probability value, its value ranges from 0 to 1. The PDF graph expresses the probability value of each event. The ordinate states the possible events, and the abscissa states the possible value $p(X)$.

$PDF = \frac{1}{\beta - \alpha}, \alpha \leq x \leq \beta$ (4)

$CDF = \frac{x - \alpha}{\beta - \alpha}, \alpha \leq x \leq \beta$ (5)

Next, we create a transfer function from the cumulative distribution of the two rainfall data using three regression functions, as in the previous method. This equation is then used as the bias correction for satellite data.

Validation of satellite rainfall data

Validation is a crucial step in assessing the accuracy and reliability of a model in predicting hydrological processes. In this study, validation was employed to assess the effectiveness of the bias correction method. Several validation

metrics were utilized, including root mean squared error (RMSE), Nash–Sutcliffe efficiency (NSE), correlation coefficient (R), and relative error (KR) [Mamenun et al., 2014; Yang et al., 2017]. Equations 6 to 9 outline the calculation procedures for these metrics.

The RMSE and relative error values indicate a high level of satellite reliability when they are close to 0. Meanwhile, the NSE and correlation coefficient values close to 1 indicate a high level of satellite reliability. These two indicators have clear parameter quantification, as depicted in Tables 1 and 2.

Root mean square error

RMSE is a standard method to measure the error of a model in predicting quantitative data. RMSE is used to evaluate the performance of a linear regression model by measuring the accuracy of the model’s estimation results. In other words, this method is used to measure how well a regression model predicts the data.

$RMSE = \sqrt{\frac{\sum_{i=1}^N (P_i - Q_i)^2}{N}}$ (6)

Nash–Sutcliffe efficiency

This method shows the degree of accuracy that results from the correlation of relationships formed between observational data and estimated data [Jarwanti et al., 2021]. This method also shows the value of whether the plot results are better than the observed values (observed data) compared to the values resulting from the prediction-simulation, whether they fit the 1:1 line

Table 1. Criteria for nash-sutcliffe efficiency

NSE	Interpretation
NSE > 0.75	Good
0.36 < NSE < 0.75	Meet the requirements
NSE < 0.36	Does not meet the requirements

Note: Motovilov et al., [1999].

Table 2. Criteria for correlation coefficient

R	Interpretation
0–0.19	Very low
0.20–0.39	Low
0.40–0.59	Moderate
0.60–0.79	High
0.80–1.00	Very high

Note: Sugiyono [2003].

or not, with a value range of ∞ to 1 [Rahma et al., 2019]. A model can be said to be good if it produces a Nash coefficient value close to one. The NSE score criteria are presented in Table 1.

$$NSE = 1 - \frac{\sum_{i=1}^N (P_i - Q_i)^2}{\sum_{i=1}^N (P_i - \bar{P})^2} \quad (7)$$

Correlation coefficient

Correlation analysis is a statistical method commonly used to determine the strength of the relationship between two variables (Table 2).

$$R = \frac{N \sum_{i=1}^N P_i - Q_i - \sum_{i=1}^N P_i \times \sum_{i=1}^N Q_i}{N \sum_{i=1}^N P_i^2 - (\sum_{i=1}^N P_i)^2 \sqrt{N \sum_{i=1}^N Q_i^2 - (\sum_{i=1}^N Q_i)^2}} \quad (8)$$

Relative error

This analysis aims to compare the magnitude of the value of one variable and another variable, which is considered as a benchmark for the actual variable [Lufi et al., 2020].

$$KR = \frac{\sum_{i=1}^N P_i - Q_i}{\sum_{i=1}^N P_i} \times 100\% \quad (9)$$

where: P_i – observation data, Q_i – forecast data (satellite data), I – average observational data, N – number of data

Rainfall projections

Rainfall projections were performed using the coupled climate models MIROC6 and MRI-ESM2-0 in the Coupled Model Intercomparison Project Phase 6 (CMIP-6) framework with the SSP2-4.5 scenario. The data used is 2023–2030. The data is in the form of average daily monthly rainfall. This data can be accessed globally via <https://esgf-node.llnl.gov/search/cmip6/> CMIP-6 output is netCDF data. RStudio was used to extract data into Microsoft Excel (.csv) format, as well as to input shapable data for the desired study area.

Water availability projections

Water availability in this study was analyzed using the Weibull probability equation by taking a discharge of 80% exceeded based on the half-monthly average discharge. Discharge data were obtained using the F.J. model simulation method. Mock. This model transforms rainfall flow following the principle of water balance [Setiyawan et al., 2017]. Existing rain data from 2010 to 2022, and projected rain data from 2023 to 30 was incorporated. CHIRPS satellite

rain data, which has previously undergone bias correction and validation, are used as input in the calculations. In addition to rain data, the model simulations of F.J. Mock also used measured discharge data from the Gowa Water Prediction Post from 2010 to 2020 to determine the groundwater recession constant) and initial groundwater storage values.

RESULT AND DISCUSSION

Observed rainfall

There are 8 rainfall stations that influence the upper rain catchment area of the Serang watershed: Juwangi, Karanggede, Simo, Sambu, Teras, Mojosoongo, Boyolali, and Ampel stations. Each rain station has varying data. From all influential rainfall stations, regional rainfall analysis was performed using arithmetic methods. Based on the results of the analysis of observational rainfall data for 16 years (2007–2022), the study area has an annual average rainfall of approximately 2.000–3.000 mm/year. Table 3 shows analysis of annual rainfall data.

Satellite rainfall

The comparison of annual rainfall data between observational and satellite sources (GPM and CHIRPS), as shown in Figure 2, indicates that both datasets exhibit similar trends or patterns. However, the rainfall amount estimated from the two satellite datasets tend to overestimate compared to the observational data.

Based on the analysis of GPM satellite rainfall data from 2007 to 2022, the study area has an average annual rainfall ranging from 1.400 to 2.100 mm/year. In contrast, CHIRPS satellite rainfall data indicates an average annual rainfall ranging from 2.100 to 4.000 mm/year. The comparison of rainfall values based on observations and those derived from GPM and CHIRPS satellite data reveals discrepancies, as illustrated in Figure 2. Generally, satellite-estimated rainfall amounts do not align with the observed rainfall data, necessitating corrections [Partarini et al., 2021]. These differences may stem from various errors, including those related to sensors (Tang et al., 2015) and retrieval algorithms [Sadeghi et al., 2019].

Table 3. Annual regional rainfall observations (2007–2022)

Year	Jan	Feb	Mar	Apr	May	Jun	Jul	Aug	Sep	Okt	Nov	Des	Annual prec.
2007	154	403	320	312	134	28	14	0	0	51	221	367	2004
2008	287	366	492	204	74	14	10	1	2	248	274	333	2304
2009	524	520	205	130	206	155	0	3	0	43	248	157	2193
2010	467	332	308	326	344	133	48	132	199	184	217	301	2990
2011	424	382	344	280	224	82	32	0	59	120	245	258	2450
2012	401	418	254	256	141	79	0	0	0	121	274	378	2322
2013	423	345	348	239	211	178	73	80	1	176	200	277	2551
2014	423	345	348	239	211	178	73	80	1	176	200	277	2551
2015	373	409	240	243	159	86	0	0	0	13	126	246	1895
2016	400	374	281	291	226	149	129	146	199	234	287	329	3045
2017	428	375	251	262	141	70	15	0	53	208	449	267	2520
2018	348	477	260	102	30	49	0	0	5	5	0	196	1474
2019	411	405	279	279	125	0	0	0	0	6	405	268	2178
2020	435	414	294	260	160	13	5	19	6	201	219	300	2326
2021	448	378	286	265	162	154	14	19	126	140	264	246	2502
2022	473	326	356	177	281	268	59	101	123	221	272	305	2962

Correction of the rainfall data

Corrections have been applied to ensure that satellite-derived rainfall data from GPM and CHIRPS exhibits a pattern identical to that of station-based observation rainfall, increasing the likelihood that it accurately represents future rainfall patterns. Corrections were needed since raindrops from the atmosphere take a certain amount of time to fall to the Earth's surface, with speeds ranging from 0.5 to 9 m/s [Marzuki et al., 2013]. Bias correction for the GPM and CHIRPS satellite rainfall data was conducted using regression and distribution mapping method, specifically through the probability density function and cumulative density function.

Bias correction through the polynomial regression method demonstrated the highest correlation compared to linear and exponential regression for both GPM and CHIRPS satellite data, as depicted in Figure 3. Polynomial regression analysis yielded R^2 values of 0.7451 for GPM and 0.7769 for CHIRPS satellite data, indicating that the polynomial method most accurately captures the relationship between observed rainfall and satellite-derived rainfall. After determining the most suitable correction equation, corrected satellite rainfall data were derived using the polynomial regression equation.

The resolution of satellite data significantly affects the efficacy of the correction factor,

evident in the varying responses between observed rainfall data corrected satellite rainfall data from GPM and CHIRPS. For GPM, the relationship between observed and corrected satellite rainfall data shows a modest improvement in the R^2 value, increasing from 0.7451 (Figure 3) to 0.7678 (Figure 4a). In contrast, the correction for CHIRPS satellite data reveals a more substantial enhancement, with the R^2 value rising from 0.7769 (Figure 3) to 0.8453 (Figure 4b). The finer spatial resolution of CHIRPS, at a grid size of $0.05^\circ \times 0.05^\circ$ compared to GPM's $0.10^\circ \times 0.10^\circ$, contributes to this difference. The higher detail offered by CHIRPS's narrower grid results in corrections that more significantly improve the accuracy of its rainfall data [Partarini et al., 2021].

GPM and CHIRPS satellite rainfall values have a high correlation value (> 0.70) with observed rainfall. However, the accuracy of satellite rain data can still be enhanced by correcting existing biases [Partarini et al., 2021]. This correction is performed using monthly data according to the equation for each month.

In comparison to the regression method, the distribution mapping method is also used to perform bias correction for GPM and CHIRPS satellite data. Linear and polynomial equations can be used in the distribution mapping method. However, you need to be careful when using linear and polynomial equations because these equations contain constant values that can cause the

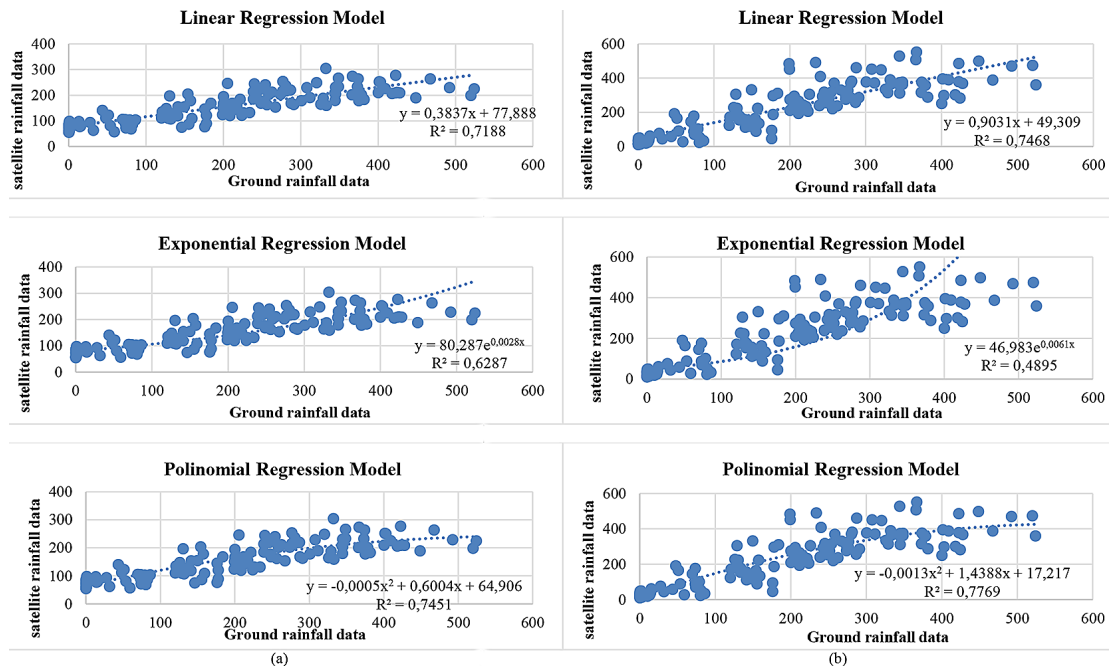


Figure 3. Bias correction of satellite rainfall data (a) GPM and (b) CHIRPS using the Regression Method

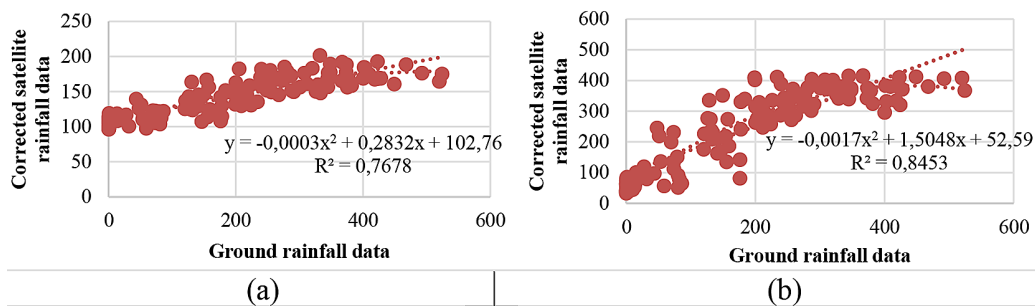


Figure 4. Relationship between observed rainfall data and corrected satellite rainfall data: (a) GPM and (b) CHIRPS

rain correction results to be illogical and negative. Therefore, this study also applies linear equations to calculate the distribution mapping method.

Bias correction of GPM and CHIRPS satellite data using the distribution mapping method shows similar R² values (Figures 5 and 6). Based on distribution mapping analysis, the relationship between observed rainfall data and GPM and CHIRPS satellite rainfall data is 0.7711 and 0.7979, respectively. In this method, the relationship between observation and satellite data is adjusted to the size of the transfer function distribution. where the transfer function value in the form of rainfall is based on the CDF value, which then causes the scatterplot graph to approach the 45° line [Partarini et al., 2021]. The relationship between these two data sets is a transfer function that is described by a linear equation for satellite data correction.

The bias correction value using the distribution mapping method on GPM and CHIRPS data is better than the correction value using the Regression method. This is indicated by the higher R² value in the distribution mapping method compared with the regression method. This shows that the most appropriate corrected rainfall value is produced using the distribution mapping method.

CHIRPS data obtained using the distribution mapping method show better results than GPM data. This can be seen from the graphic display of both the PDF and CDF from CHIRPS, which almost coincide with the observation data, whereas in GPM, both the PDF and CDF graphs show deviations between the observation and satellite data (Figures 5 and 6). This shows that CHIRPS data are more in agreement with observational data than with GPM data.

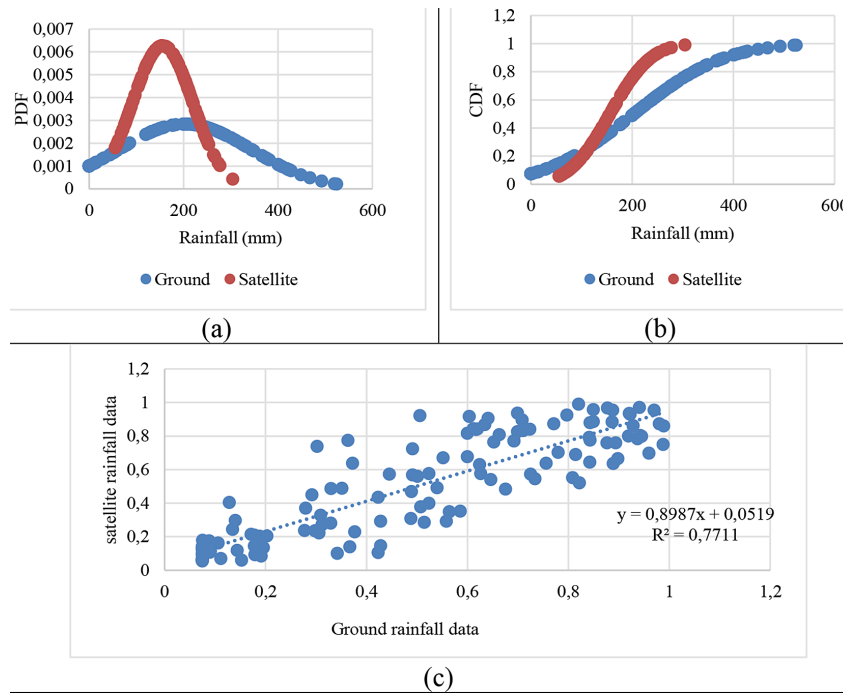


Figure 5. Comparison of (a) PDF and (b) CDF curves and (c) Bias correction between observed rain data and GPM satellite rain data using the distribution mapping method

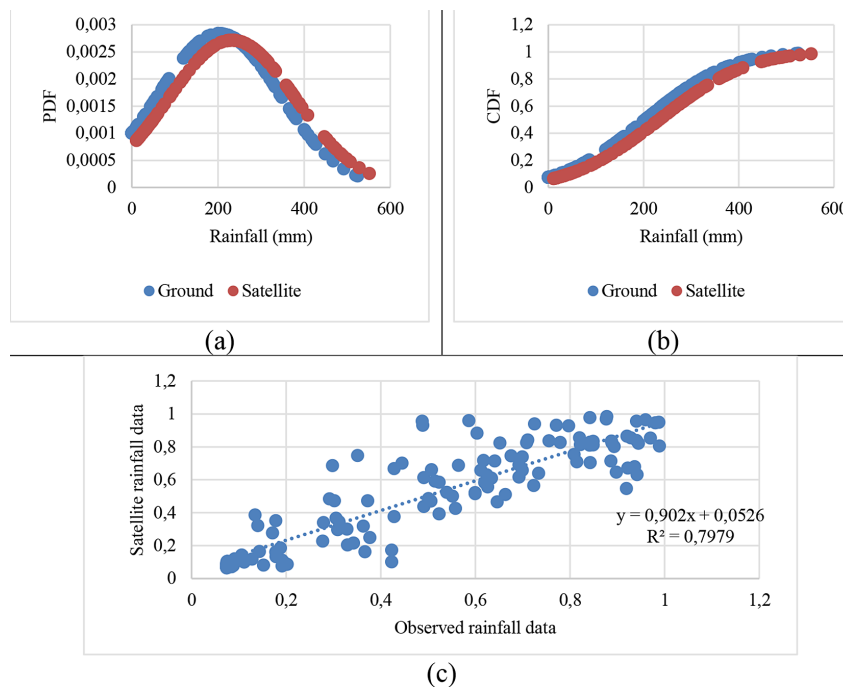


Figure 6. Comparison of (a) PDF and (b) CDF curves and (c) Bias correction between observed rainfall data and CHIRPS satellite rainfall data using the distribution mapping method

Corrected satellite rainfall data produced from the GPM and CHIRPS data show different results. Based on the bias correction results, the corrected satellite data in CHIRPS show significant changes compared with the uncorrected satellite data. The corrected satellite data in CHIRPS

almost coincide with the observed rainfall data (Figure 8). This means that the corrections made to the initial satellite data were successful because the resulting corrected values were close to the observed values. This indicates that the correction factor makes the predicted value have

the same rainfall distribution pattern as the observed rainfall. Different things are shown by the corrected satellite data on GPM. The corrected GPM satellite rainfall data are not much different from the satellite data before correction. Corrected satellite rain data on GPM still has a long range compared with observed rain data (Figure 7). This means that the corrections made to the initial satellite data were unsuccessful because the resulting corrected values were still far from the observed values. Supposedly, the correction factor causes the predicted value to have the same rainfall distribution pattern as the observed rainfall [Partarini et al., 2021]. It can be concluded that the corrected CHIRPS satellite data shows better results than the GPM corrected satellite

data because it produces patterns that are in accordance with observed rainfall in describing the influence of climate change. Therefore, corrected CHIRPS satellite data will be used for the water availability prediction stage. Based on the accuracy between the two bias correction methods, the distribution mapping method produces satellite rainfall data that is more similar than the data corrected by the regression method. This shows that the most suitable rainfall value is generated from the distribution mapping corrected satellite data.

Validation of the rainfall data

Validation is used to evaluate the bias correction method. In this study, validation was performed

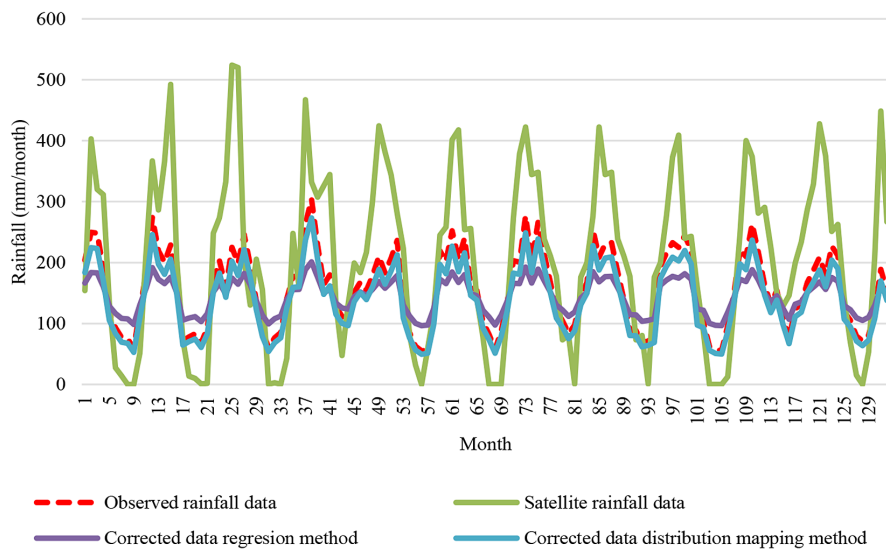


Figure 7. Comparison of the bias correction of GPM satellite data

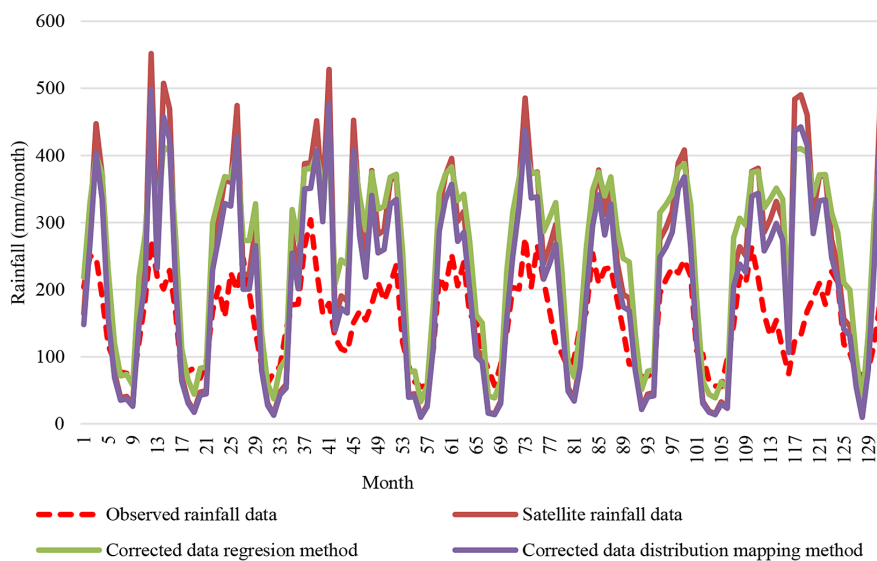


Figure 8. Comparison of the bias correction of CHIRPS satellite data

using four statistical methods in the form of objective functions, including root mean squared error, Nash–Sutcliffe efficiency, correlation coefficient I, and relative error. For data with corrections, validation is generally performed using data outside the data period used in the calibration stage [Indarto, 2012]. Therefore, validation of satellite rainfall data (GPM and CHIRPS) was carried out over a period of 5 years, namely 2018–2022. The suitability of the validation is based on the RMSE, NSE, KR, and R values obtained (Tables 4 and 5).

By paying attention to the results of the four validation methods, it can be determined that the most appropriate correction method for both GPM and CHIRPS satellite rainfall data is the same, namely the distribution mapping method. This is based on both satellite data. The RMSE value for the distribution mapping method is the lowest and the relative error is also the lowest indicating that the results are accurate. This is supported by the highest NSE value, and the correlation coefficient is strong. The resulting values for RMSE, NSE, R, and KR for the GPM satellite are 120.76, 0.348, 0.856, and 29.985, respectively, while for the CHIRPS satellites it is 105.21, 0.504, 0.80, and 26.058, respectively (see Tables 4 and 5). Differences in validation results can be influenced by the length of the calibration and validation data used [Partarini et al., 2021].

Low RMSE and KR values provide better results because they indicate a low error rate [Amelia et al, 2021]. The smaller the RMSE value, the smaller the difference between the two, so the results of the satellite estimated values

will be more accurate [Jarwanti et al., 2021]. Meanwhile, NSE and R values that are close to 1 are better because they show a high level of reliability between the observed and modeled data. NSE and R have clear parameter quantification to show the level of accuracy, which is better the closer it is to 1 [Jarwanti et al., 2021]. Therefore, it can be concluded that the distribution mapping method produces better validation values than other methods. However, when comparing GPM and CHIRPS, the analysis results show that CHIRPS satellite data are better than GPM satellite data. This can be seen from the RMSE, NSE, and R values. The relative error value in CHIRPS rain data is relatively lower than that in GPM data.

Projection of the rainfall

The projected rainfall is used to predict water availability in the coming year. In this study, projected rainfall was conducted to obtain monthly rainfall data from 2023 to 2030. Using coupled climate modeling MIROC6 and MRI-ESM2-0 in the CMIP-6 framework, projected rainfall data can be obtained as shown in Table 6.

MIROC6 and MRI-ESM2.0 are used in the CMIP-6 framework because they have good accuracy in projecting rain data. MIROC6 was initialized by assimilating observed ocean temperature and salinity anomalies as well as sea ice concentration so that it can predict surface temperatures better than MIROC5 and the annual average sea surface temperature in the North Atlantic, North

Table 4. Results of bias correction validation of GPM satellite rain data for year 2018–2022

Bias correction methods		Validation methods			
		RMSE	R	NSE	KR
Observation data	Non corrected	120.35	0.856	0.352	29.691
Regression methods	Linear	145.43	0.856	0.054	32.175
	Polynomial	149.67	0.856	0.312	36.390
Distribution mapping method	PDF	120.76	0.856	0.348	29.985

Table 5. Results of bias correction validation of CHIRPS satellite rain data for year 2018–2022

Bias correction methods		Validation methods			
		RMSE	R	NSE	KR
Observation data	Non corrected	129.41	0.80	0.251	-38.36
Regression methods	Linear	138.09	0.80	0.147	-50.82
	Polynomial	109.35	0.85	0.466	-39.01
Distribution mapping method	PDF	105.21	0.80	0.504	26.058

Pacific, and Eastern tropical Pacific [Kataoka et al., 2020]. Similar to MRI-ESM2.0, [Yukimoto et al., 2019] stated that the new Meteorological Research Institute Earth System Model version 2.0 (MRI-ESM2.0) has many improvements for very accurate climate reproducibility. The model is capable of providing a realistic reproduction of climate means and interannual variability. Furthermore, [Kawai et al., 2019] stated that MRI-ESM2.0 can provide significant improvements in cloud representation. Therefore, the resulting projections are more accurate. Rainfall projections (Table 6) were used to predict water availability in the coming year.

Water availability predictions for conservation strategy

The results of the observational and satellite rain projections exhibit an identical trend. This certainly influences the predictions of water availability in the coming period. Calculation of water availability predictions is performed using the Weibull probability equation by taking a discharge of 80% or an andaman discharge exceeded

based on the half-monthly average discharge modeled using the F.J. method. Mock (see methods). Radhika et al. [2017] stated that the low level of discharge measurement data has resulted in doubts about the quality of river flow discharge data. Therefore, studies of river flow discharge at water estimation posts must consider rainfall and climate data to produce figures that are not too high [Radhika et al., 2017]. Based on prediction results through the mainstay debit (Q80), in the wet months, namely January–May and November–December, monthly water availability ranges from 16.01 to 45.28 m³/s, whereas in the dry months, namely June–October, monthly water availability ranges from 5.70 to 25.87 m³/s (Table 7). Monthly water availability predictions were then used to predict annual water availability (Figure 9). Based on annual data processing, the graph shows that water availability for the coming period (2023–2030) will generally show an increase. The decrease in the graph shows a decrease in water availability that is not too significant, around 1–2 m³/s. The most drastic increase will occur in 2028–2029, when water availability will increase by approximately 10 m³/s.

Table 6. Rainfall projection for the study area for 2023–2030

Year	Jan	Feb	Mar	Apr	May	Jun	Jul	Aug	Sep	Oct	Nov	Dec
2023	21.50	27.81	10.33	17.87	12.26	2.42	0.54	0.53	0.32	9.16	21.47	3.94
2024	20.92	22.08	19.87	14.65	7.14	0.33	3.25	3.15	7.81	19.90	16.82	5.93
2025	13.27	23.50	10.98	8.78	6.00	3.51	6.57	11.18	13.45	22.27	12.57	12.11
2026	12.84	19.60	9.73	13.89	6.86	3.81	7.29	9.59	6.05	10.42	21.70	13.59
2027	14.97	19.03	9.19	4.15	6.96	5.36	5.59	7.64	11.95	12.69	8.96	18.92
2028	20.41	17.79	9.62	19.31	4.71	2.03	1.02	0.84	2.33	6.98	15.30	11.78
2029	15.32	5.90	17.06	11.83	17.86	2.37	8.67	13.27	21.09	27.35	17.25	26.20
2030	9.26	19.80	12.46	12.64	7.74	12.18	5.04	16.67	21.96	20.95	16.80	23.34

Table 7. Prediction of monthly water availability based on yearly rainfall predictions 2023–2030

Year	2010–2030 (%)	Jan		Feb		Mar		Apr		May		Jun		Jul		Aug		Sep		Oct		Nov		Dec	
		I	II	I	II	I	II	I	II	I	II	I	II	I	II	I	II								
2023	63.6	25.0	30.4	33.7	31.4	29.1	25.4	24.3	22.4	17.9	10.1	7.7	5.6	4.6	4.3	2.3	1.7	4.0	4.4	6.3	14.8	21.0	23.8	24.9	21.3
2024	68.2	22.9	29.0	32.8	30.8	28.2	22.8	19.8	21.8	17.7	8.4	6.3	5.6	3.9	3.8	2.2	1.6	3.9	3.4	5.9	12.0	20.5	23.3	24.1	21.2
2025	72.7	20.4	28.2	31.5	29.3	26.0	19.8	17.8	21.1	17.4	8.3	5.6	5.3	3.5	2.7	1.7	1.6	3.0	3.3	4.8	11.9	20.4	22.8	23.9	20.6
2026	77.3	18.3	26.8	29.7	27.9	25.3	19.6	16.6	19.8	16.6	7.9	5.5	4.6	2.4	2.3	1.6	1.5	1.4	3.1	3.1	11.1	20.1	17.9	22.6	16.1
2027	81.8	16.3	26.1	27.1	27.8	23.9	17.2	16.3	18.8	16.1	5.9	5.1	2.8	2.2	2.1	1.4	1.2	1.0	2.4	1.9	7.4	18.1	15.5	21.1	13.2
2028	86.4	13.8	26.1	26.3	25.4	20.2	14.2	15.3	15.8	13.7	5.9	4.7	2.6	1.9	1.0	0.5	0.6	0.7	2.0	1.7	5.2	17.1	15.3	18.4	13.1
2029	90.9	13.2	25.2	23.9	23.2	13.7	13.8	12.6	15.1	6.9	5.6	4.6	2.5	1.8	1.0	0.5	0.2	0.1	1.0	1.7	3.7	16.3	11.0	13.4	12.2
2030	95.5	11.9	21.5	10.8	16.2	12.6	12.7	7.0	8.9	6.8	4.8	3.6	2.2	1.0	1.0	0.4	0.2	0.1	0.1	1.5	2.2	10.9	7.8	10.6	11.8
Q (m ³ /s)	80	19.3	20.5	28.7	25.8	45.2	45.3	34.8	16.0	29.9	11.2	7.7	5.7	10.8	6.2	25.9	6.5	8.2	35.2	8.3	15.3	18.1	23.7	16.6	27.6

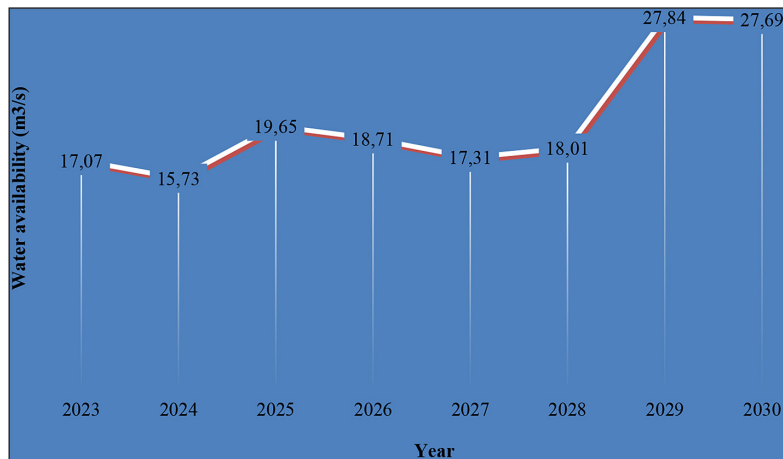


Figure 9. Prediction of annual water availability year 2023–2030

The increase in water availability in 2028–2029 for about 10 m³/s describes that conservation strategies are needed to anticipate excess water in cultivated land. Methods that can be conducted to control water as needed for plants include reducing water loss through retention ponds in cultivated land; and improving water management techniques such as regulating the drainage system.

CONCLUSIONS

The analysis demonstrated that CHIRPS was outperform GPM rainfall data. Distribution Mapping method showed better results for bias correction compared to Regression method, and it further enhances the accuracy of satellite rainfall data. The differences observed in validation results may be attributed to the duration of calibration and validation datasets. Predictions of rainfall using satellite data offer valuable inputs for water availability forecasting for agricultural needs and serve as a preliminary framework for conservation strategy in response to water deficits or surpluses in agriculture. A significant advantage of this satellite-based analysis is its ability to determine surface water potential across any location in Indonesia by calculating the product of the catchment area's size and runoff height.

Acknowledgements

The author would like to thank to Department of Soil, Faculty of Agriculture, Universitas Gadjah Mada to support the presentation of this paper draft in Indonesian Soil Science Congress 2023 for gaining many inputs and suggests from other colleagues before it is submitted.

REFERENCES

- Collischonn, B., Collischonn, W., Tucci, C.E.M. 2008. Daily hydrological modeling in the Amazon basin using TRMM rainfall estimates. *Journal of Hydrology*, 360(1–4), 207–216. <https://doi.org/10.1016/j.jhydrol.2008.07.032>
- Chellamuthu, S.N., Ganapathy, G.P., 2024. Quantifying the impact of changing rainfall patterns on landslide frequency and intensity in the Nilgiris District of Western Ghats, India, *Progress in Disaster Science*, 3 <https://doi.org/10.1016/j.pdisas.2024.100351>
- Damayanti, A.C., Limantara, L.M., Haribowo, R. 2022. Analisis debit banjir rancangan dengan metode HSS Nakayasu, HSS ITB-1, dan HSS Limantara pada DAS Manikin di Kabupaten Kupang. *Jurnal Teknologi Dan Rekayasa Sumber Daya Air*, 2(2), 313. <https://doi.org/10.21776/ub.jtresda.2022.002.02.25>
- Dwiratna N.P.S., Nawawi, G. dan Asdak, C. 2014. Analisis curah hujan dan aplikasinya dalam penetapan jadwal dan pola tanam pertanian lahan kering di Kabupaten Bandung. *Bionatura-Jurnal Ilmu-Ilmu Hayati Dan Fisik*, 16(2), 95–102.
- Fadholi, A., Sari, F.P., Aji, P., Dewi, R. 2014. Pemanfaatan model Weather Research and Forecasting (WRF) dalam Analisis Cuaca terkait Hujan Lebat Batam 30-31 Januari 2011. *Jurnal Fisika Dan Aplikasinya*, 10(1), 24. <https://doi.org/10.12962/j24604682.v10i1.820>
- Fadli, D.M. 2022. Pemanfaatan data satelit terhadap prediksi curah hujan. *Jurnal Konstruksi*, 20(1), 194–201. <https://doi.org/10.33364/konstruksi/v.20-1.1107>
- Fauzi, M., Darmayanti, L., Hilwan, F. 2013. Pengisian Kekosongan Data Hujan Dengan Metode Multiple Nonlinier Standardize Corelation Pada Stasiun Hujan Daerah Aliran Sungai Indragiri Dan Rokan.

- Semantic Scholar, 2, 1–7.
8. Haddeland, I., Heinke, J., Biemans, H., Eisner, S., Flörke, M., Hanasaki, N., Konzmann, M., Ludwig, F., Masaki, Y., Schewe, J., Stacke, T., Tessler, Z.D., Wada, Y., Wisser, D. 2014. Global water resources affected by human interventions and climate change. *Proceedings of the National Academy of Sciences of the United States of America*, 111(9), 3251–3256. <https://doi.org/10.1073/pnas.1222475110>
 9. Haslinger, K., Koffler, D., Schoner, W., Laaha, G. 2014. Exploring the link between meteorological drought and streamflow: Effects of climate-catchment interaction. *Water Resources Research*, 5375–5377. <https://doi.org/10.1002/2013WR014979>.Reply
 10. Hasyimzoem, E.F., Zakaria, A., Sumiharni. 2021. Perbandingan analisis data curah hujan yang hilang menggunakan metode normal ratio, inversed square distance, Rata-Rata Al-jabar, dan Regresi Berganda. *Jurnal Rekayasa Sipil*, 7(1), 155–162. <http://journal.eng.unila.ac.id/index.php/jrsdd/article/view/1322>
 11. Indarto, I. 2012. Prosedur kalibrasi dan validasi model SMAR untuk mendeskripsikan proses hujan aliran di Sub-DAS Rawatantu. *Jurnal Teknik Sipil*, 19(3), 265. <https://doi.org/10.5614/jts.2012.19.3.7>
 12. Jarwanti, D.P., Suhartanto, E., Fidari, J.S. 2021. Validasi data curah hujan satelit TRMM (Tropical Rainfall Measuring Mission) dengan data pos penakar hujan di DAS Grindulu, Kabupaten Pacitan, Jawa Timur. *Jurnal Teknologi Dan Rekayasa Sumber Daya Air*, 1(2), 772–785.
 13. Kataoka, T., Tatebe, H., Koyama, H., Mochizuki, T., Ogochi, K., Naoe, H., Imada, Y., Shiogama, H., Kimoto, M., Watanabe, M. 2020. Seasonal to decadal predictions with MIROC6: description and basic evaluation. *Journal of Advances in Modeling Earth Systems*, 12(12), 1–25. <https://doi.org/10.1029/2019MS002035>
 14. Kawai, H., Yukimoto, S., Koshiro, T., Oshima, N., Tanaka, T., Yoshimura, H., Nagasawa, R. 2019. Significant improvement of cloud representation in the global climate model MRI-ESM2. *Geoscientific Model Development*, 12(7), 2875–2897. <https://doi.org/10.5194/gmd-12-2875-2019>
 15. Laimheeriwa, S., Pangaribuan, M., Amba, M. 2019. analisis fenomena El Nino dan dampaknya terhadap neraca air lahan di pulau Ambon. *Jurnal Budidaya Pertanian*, 15(2), 111–118. <https://doi.org/10.30598/jbdp.2019.15.2.111>
 16. López-Moreno, J.I., Zabalza, J., Vicente-Serrano, S.M., Revuelto, J., Gilaberte, M., Azorin-Molina, C., Morán-Tejeda, E., García-Ruiz, J.M., Tague, C. 2014. Impact of climate and land use change on water availability and reservoir management: Scenarios in the Upper Aragón River, Spanish Pyrenees. *Science of the Total Environment*, 493, 1222–1231. <https://doi.org/10.1016/j.scitotenv.2013.09.031>
 17. Lorenzo-Lacruz, J., Vicente-Serrano, S.M., González-Hidalgo, J.C., López-Moreno, J.I., Cortesi, N. 2013. Hydrological drought response to meteorological drought in the Iberian Peninsula. *Climate Research*, 58(2), 117–131. <https://doi.org/10.3354/cr01177>
 18. Mamenun, Pawitan, H., Sophaheluwakan, A. 2014. Validasi dan koreksi data satelit TRMM pada tiga pola hujan di Indonesia (Validation and correction of TRMM satellite data on three rainfall patterns in Indonesia). *Jurnal Meteorologi Dan Geofisika*, 15(1), 13–23. <http://202.90.199.54/jmg/index.php/jmg/article/view/169/155>
 19. Marzuki, Randeu, W.L., Kozu, T., Shimomai, T., Hashiguchi, H., Schönhuber, M. 2013. Raindrop axis ratios, fall velocities and size distribution over Sumatra from 2D-Video Disdrometer measurement. *Atmospheric Research*, 119, 23–37. <https://doi.org/10.1016/j.atmosres.2011.08.006>
 20. Misnawati, M., Boer, R., June, T., Faqih, A. 2018. perbandingan metodologi koreksi bias data curah hujan CHIRPS. *Limnotek*, 25(1), 18–29.
 21. Ouharba, E.H., Mabrouki, J., Triqui, Z.E.A., 2024. Assessment and future climate dynamics in the Bouregreg Basin, Morocco - Impacts and adaptation alternatives. *Ecol. Eng. Environ. Technol.* 25(3), 51–63 <https://doi.org/10.12912/27197050/177823>
 22. Partarini, N.M.C., Sujono, J., Pratiwi, E.P.A. 2021. Koreksi dan Validasi data curah hujan satelit GPM-IMERG dan CHIRPS di Das Selorejo, Kabupaten Malang. *Prosiding CEEDRiMS*, 1(1), 149–156. <https://giovanni.gsfc.nasa.gov/>
 23. Putri, D., Perdinan. 2018. Analysis of regional water availability for domestic water demand (Case Study: Malang Regency). *Agromet*, 32(2), 93. <https://doi.org/10.29244/j.agromet.32.2.93-102>
 24. Radhika, Fauzi, M., Rahmawati, S., Rendy, F., Anthon, F., Hatmoko, W. 2012. Neraca ketersediaan air permukaan dan kebutuhan air pada wilayah sungai di Indonesia. *Kolokium Hasil Penelitian Dan Pengembangan Sumber Daya Air*, 193, 1–14.
 25. Radhika, R., Firmansyah, R., Hatmoko, W. 2017. Perhitungan ketersediaan air permukaan di Indonesia berdasarkan data satelit. *Jurnal Sumber Daya Air*, 13(2), 115–130. <https://doi.org/10.32679/jsda.v13i2.206>
 26. Ramzi, K., Nadir, M., Tewfik, B.M., Hakim, D.K. 2024. Hydrological forecasts modeling using artificial intelligence and conceptual models of Kébir-Rhumel Watershed, Algeria, *Ecol. Eng. Environ. Technol.* 25(9), 68–80.
 27. Rahma, N.F., Suhartanto, E., Harisuseno, D. 2019. Validasi data curah hujan TRMM (Tropical Rainfall Measuring Mission) dengan Pos Stasiun Hujan di Sub DAS Sumber Brantas. *Jurnal Mahasiswa Teknik Pengairan Universitas Brawijaya*, 2(2), 1–13.
 28. Romadhoniastri, S., Ayumi, N., Ulumia, F., Zahro,

- N.A., Rahayuli, R., Wahyudi, R., Hayat, D.M., Hadi, M.P. 2022. Kajian karakteristik aliran sungai serang di AWLR bendungan kulonprogo berdasarkan pemodelan hidrologi HEC-HMS. *Jurnal Geografi : Media Informasi Pengembangan Dan Profesi Kegeografian*, 19(2), 54–61. <https://doi.org/10.15294/jg.v19i2.33671>
29. Stodolak, R., Baran, J., Knap, E., 2018. The influence of rain temopration on the results of rainfall-runoff model. *Inż. Ekolog.* 19(6), 87–93 <https://doi.org/10.12912/23920629/95271>
30. Sadeghi, M., Asanjan, A.A., Faridzad, M., Nguyen, P.H.U., Hsu, K., Sorooshian, S., Braithwaite, D.A.N. 2019. PERSIANN-CNN: Precipitation estimation from remotely sensed information using artificial neural networks–convolutional neural networks. *Journal of Hydrometeorology*, 20(12), 2273–2289. <https://doi.org/10.1175/JHM-D-19-0110.1>
31. Setiyawan, Andiese, V.W., Anzar, L.A. 2017. Analisis ketersediaan air dengan metode F.J mock pada daerah persawahan desa Poboya Palu Sulawesi Tengah. *Infrastruktur*, 7(1), 18–26.
32. Simanjuntak, J.T., Azka, M.A., Dzikiro, T.K., Hariadi. 2018. Analisis dampak fenomena El Nino terhadap ketersediaan air tanah di Bima, NTB Pada Tahun 2015. *Seminar Nasional Pelestarian Lingkungan*, May, 187–193.
33. Susanti, E., Surmaini, E., Pramudia, A., Heryani, N., Estiningtyas, W., Suciantini, S., Apriyana, Y. 2021. Pemutakhiran peta sumberdaya agroklimat indonesia untuk mendukung perencanaan pertanian. *Jurnal Tanah Dan Iklim*, 45(1), 47. <https://doi.org/10.21082/jti.v45n1.2021.47-58>
34. Tabari, H. 2020. Climate change impact on flood and extreme precipitation increases with water availability. *Sci Rep* 10, 13768. <https://doi.org/10.1038/s41598-020-70816-2>
35. Tavosi, M., Vafakhah, M., Shekohideh, M., Sadeghi, S., Moosavi, V., Zheng, Z., Yang, Q., 2024. Rainfall extreme indicators trend and meteorological drought changes under climate change scenarios, *Water Resources Management* <https://doi.org/10.1007/s11269-024-03871-3>
36. Tang, L., Tian, Y., Yan, F., Habib, E. 2015. An improved procedure for the validation of satellite-based precipitation estimates. *Atmospheric Research*, 163, 61–73. <https://doi.org/10.1016/j.atmosres.2014.12.016>
37. Tanzeeba, S., Gan, T.Y. 2012. Potential impact of climate change on the water availability of South Saskatchewan River Basin. *Climatic Change*, 112(2), 355–386. <https://doi.org/10.1007/s10584-011-0221-7>
38. Triyanto, S., Sunyoto, A., Arief, M.R. 2021. Analisis klasifikasi bencana banjir berdasarkan curah hujan menggunakan algoritma naïve Bayes. *JOISIE (Journal Of Information Systems And Informatics Engineering)*, 5(2), 109–117. <https://doi.org/10.35145/joisie.v5i2.1785>
39. Wu, D., Chen, J., Xiong, L., Lee, J., Kim, J., Moon, H., 2024. Assessing global drought conditions under climate change: A comparison of stationary and non-stationary approaches and identification of hotspot regions, *Journal of Hydrology*, 640, <https://doi.org/10.1016/j.jhydrol.2024.131663>
40. Yang, N., Zhang, K., Hong, Y., Zhao, Q., Huang, Q., Xu, Y., Xue, X., Chen, S. 2017. Evaluation of the TRMM multisatellite precipitation analysis and its applicability in supporting reservoir operation and water resources management in Hanjiang basin, China. *Journal of Hydrology*, 549, 313–325. <https://doi.org/10.1016/j.jhydrol.2017.04.006>
41. Yukimoto, S., Kawai, H., Koshiro, T., Oshima, N., Yoshida, K., Urakawa, S., Tsujino, H., Deushi, M., Tanaka, T., Hosaka, M., Yabu, S., Yoshimura, H., Shindo, E., Mizuta, R., Obata, A., Adachi, Y., Ishii, M. 2019. The meteorological research institute Earth system model version 2.0, MRI-ESM2.0: Description and basic evaluation of the physical component. *Journal of the Meteorological Society of Japan*, 97(5), 931–965. <https://doi.org/10.2151/jmsj.2019-051>